Structure 14, 1623–1632, November 2006 ©2006 Elsevier Ltd All rights reserved DOI 10.1016/j.str.2006.08.014

Purification and 3D Structural Analysis of Oligomeric Human Multidrug Transporter ABCG2

Christopher A. McDevitt,[1,4] Richard F. Collins,[2,4] Michael Conway,[1] Szabolcs Modok,[1] Janet Storm,[1] Ian D. Kerr,[3] Robert C. Ford,[2] and Richard Callaghan[1,*]

[1] Nuffield Department of Clinical Laboratory Sciences
John Radcliffe Hospital
University of Oxford
Oxford, OX3 9DU
United Kingdom

[2] Faculty of Life Sciences
University of Manchester
P.O. Box 88
Sackville Street
Manchester, M60 1QD
United Kingdom

[3] Centre for Biochemistry and Cell Biology
School of Biomedical Sciences
University of Nottingham
Queen's Medical Centre
Nottingham, NG7 2UH
United Kingdom

Summary

ABCG2 is a multidrug efflux pump associated with resistance of cancer cells to a plethora of unrelated drugs. ABCG2 is a "half-transporter," and previous studies have indicated that it forms homodimers and higher oligomeric species. In this manuscript, electron microscopic structural analysis directly addressed this issue. An N-terminal hexahistidine-tagged ABCG2^{R482G} isoform was expressed to high levels in insect cells. An extensive detergent screen was employed to effect extraction of ABCG2^{R482G} from membranes and identified only the fos-choline detergents as efficient. Soluble protein was purified to >95% homogeneity by a three-step procedure while retaining the ability to bind substrates. Cryonegative stain electron microscopy of purified ABCG2^{R482G} provided 3D structural data at a resolution of ~18 Å. Single-particle analysis revealed that the complex forms a tetrameric complex (~180 Å in diameter × ~140 Å high) with an aqueous central region. We interpret the tetrameric structure as comprising four homodimeric ABCG2^{R482G} complexes.

Introduction

Resistance to chemotherapy remains an unconquered and considerable barrier to the treatment of cancer. One of the most widespread factors is reduced drug accumulation by active extrusion mechanisms such as the ATP Binding Cassette (ABC) transporters. The first discovered was P-glycoprotein (ABCB1), and it has been implicated most strongly in the resistance of leukemia. In contrast, ABCC1 (MRP1), and not ABCB1, has been shown to confer resistance to chemotherapeutic agents in small-cell lung cancer cell lines. Similarly, investigations with cell lines highly resistant to mitoxantrone or daunomycin discovered the presence of a third multidrug transporter, ABCG2 (BCRP or MXR). These three ABC proteins play a pivotal role in resistance of cancer cells to an extraordinary array of anticancer agents and are known as multidrug transporters due to the promiscuity of their substrate interactions.

ABCG2 has been classified to the G subfamily of ABC transporters, all of which are considered "half-transporters" and comprise one nucleotide-binding domain (NBD) and a single transmembrane domain (TMD) containing six predicted membrane-spanning segments. The most distinguishing sequence feature of the ABCG family is the distinct topology. While the majority of ABC transporters comprise a TMD followed by a C-terminal NBD, the ABCG2 protein has an apparent "reversed structure," with the NBD located N-terminal to the TMD. These structural differences are in stark contrast to the more extensively characterized ABCB1 and ABCC1 multidrug transporters and serve to underlie the importance of ABCG2 structural studies.

ABCG2 has been directly demonstrated to confer resistance to mitoxantrone (Nakagawa et al., 1992), methotrexate (Chen et al., 2003), and camptothecin derivatives (Robey et al., 2001). Additional studies with drug-selected cultured cell lines have identified three different isoforms of ABCG2, with mutations near the third predicted transmembrane segment localized at residue 482 (Mitomo et al., 2003; Ozvegy et al., 2002). The wild-type protein contains an arginine residue, whereas the two most commonly observed mutations are either glycine or threonine. The glycine is a gain-of-function mutation in that resistance to anthracyclines, such as daunomycin and doxorubicin, is conferred and the protein is able to transport Rhodamine 123, although a loss of function with respect to methotrexate is also observed. The reason for the alteration of function has yet to be resolved, and translocated compounds, including the anthracyclines, Rhodamine 123, and camptothecins, are also substrates of ABCB1. However, not all ABCB1 substrates, such as vinblastine and calcein-AM, are recognized by ABCG2. Recent radioligand-binding data have identified the presence of multiple, pharmacologically distinct sites on ABCG2 for drug interaction (Clark et al., 2006). However, the precise nature of these sites and their location within the TMDs has not yet been determined, and there are few selective inhibitors for the protein.

The minimal functional oligomer of ABCG2 has been suggested to be a homodimer, a form necessary if it is to function as an ATP-dependent drug transporter, and several lines of evidence support this hypothesis. First, a large body of evidence from ABC transporters exists and demonstrates that two functional NBDs are required to support substrate translocation. Structural analyses with either isolated NBDs or bacterial ABC proteins, including the MsbA homodimer, have revealed that bound ATP interacts with elements (P loop and

*Correspondence: richard.callaghan@ndcls.ox.ac.uk
[4] These authors contributed equally to this work.

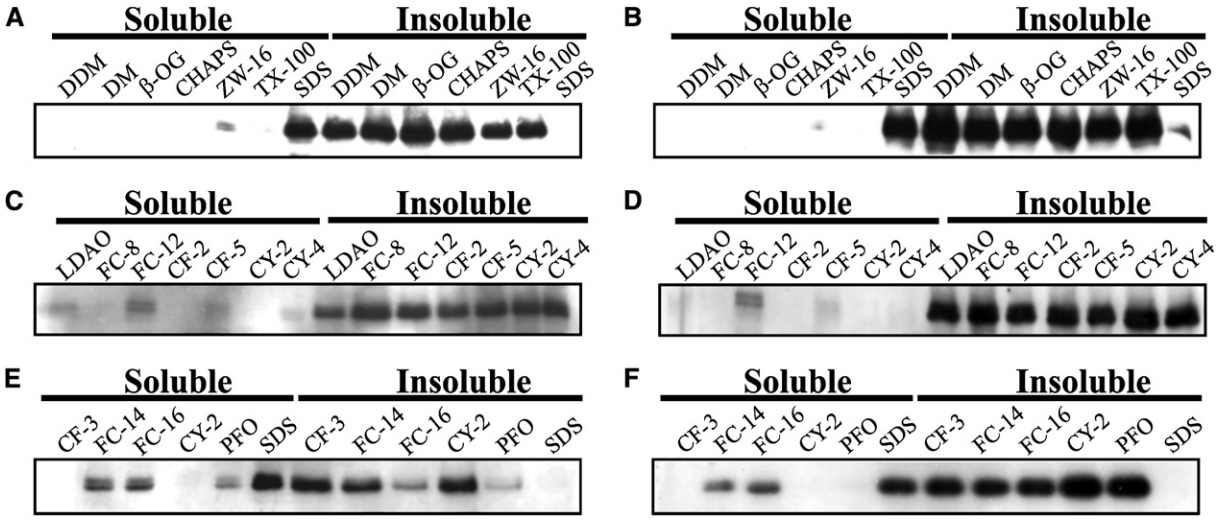

Figure 1. Efficiency of ABCG2^{R482G} Solubilization by a Range of Nonionic and Zwitterionic Detergents

(A–F) Detergent solubilization of ABCG2^{R482G} membranes was performed as described in the Experimental Procedures and was assessed by immunoblotting of the soluble and insoluble material. Detergents are shown above the sample lanes, and each fraction represented 10% of the sample. (A), (C), and (E) were obtained with membranes at a concentration of 1 mg·ml^{-1}, while (B), (D), and (F) correspond to 10 mg·ml^{-1} total membrane protein.

signature sequence) provided by each of the two NBDs (Reyes and Chang, 2005). Also, it has been established that two G subfamily members, ABCG5/ABCG8, heterodimerize to enable cholesterol efflux, and that their interaction is essential for correct localization of the proteins to the plasma membrane compartment (Graf et al., 2003).

Studies characterizing ABCG2 function have pointed to a potential for protein-protein interactions, which have been suggested to be maintained by disulfide bond formation (Kage et al., 2002; Litman et al., 2002). However, other intermolecular interactions, such as those involving the established GXXXG transmembrane helix interaction motif (Russ and Engelman, 2000), have also been implicated (Polgar et al., 2004). Recent evidence gathered from sucrose density gradient sedimentation studies has suggested that while homodimerization is abundant, there is no clear dependence on disulfide bond formation (Xu et al., 2004). Full-length transporters such as ABCB1 (Poruchynsky and Ling, 1994) and ABCC1 (Rosenberg et al., 2001; Soszynski et al., 1998) have also been suggested to form oligomeric structures, although the functional significance has not yet been elucidated, unlike that of SUR1-Kir6.2 oligomerization (Mikhailov et al., 2005), which is critical in mediating potassium conductance.

In the present manuscript, an extraction and purification procedure has been developed to enable further functional and structural analysis of the ABCG2^{R482G} transporter. The protein proved difficult to extract with commonly used detergents and ultimately required the use of fos-choline-16. Drug-binding studies demonstrate that purified protein is capable of specific interaction with transport substrates. An initial structure for ABCG2^{R482G} is presented for the purified protein by using electron microscopy, which indicates that a tetrameric complex with an aqueous central region is formed. We interpret the tetrameric structure as comprising four homodimeric ABCG2^{R482G} complexes.

Results

Solubilization of ABCG2^{R482G} from High Five Insect Cells

Recombinant baculovirus containing either the carboxy-terminal or amino-terminal hexahistidine-tagged constructs for ABCG2^{R482G} were transfected into High Five cells. Immunoblot analysis of expression levels of the two constructs on crude membranes (not shown) demonstrated a significantly higher level of expression of the amino-terminal-tagged ABCG2^{R482G}. Binding studies conducted on crude membranes (Clark et al., 2006) demonstrated functional interaction with published substrates only in the case of the amino-terminally tagged construct.

Solubilization Screen for ABCG2^{R482G}

Crude membrane preparations from the infected insect cells were tested with a range of common nonionic detergents and zwitterionic detergents to investigate the extraction conditions of ABCG2^{R482G}. The initial screen (Figures 1A and 1B) showed no extraction with any detergent other than the strong ionic detergent SDS. Lack of extraction with the glucoside- and maltoside-based detergents indicated that nonionic detergents were not cogent extractors. The zwitterionic detergents, lauryldimethylamine oxide (LDAO), fos-choline (FC), and cyclofos (CF), as well as the nonionic cymal series (CY), were screened. Figures 1C and 1D demonstrate weak extraction of ABCG2^{R482G} by LDAO, FC-12, and CF-5. In contrast to FC-12, FC-8's failure to liberate the protein suggested that the length of the alkyl chain of the detergent may be important in its ability to extract ABCG2^{R482G}. Longer chain length variants of the FC detergents were screened in addition to a number of other conditions (Figures 1E and 1F). Both FC-14 and FC-16 showed extraction irrespective of the protein concentrations used, while pentadecafluoro-octanoic acid (PFO) only showed relatively weak extraction at 1 mg·ml^{-1}.

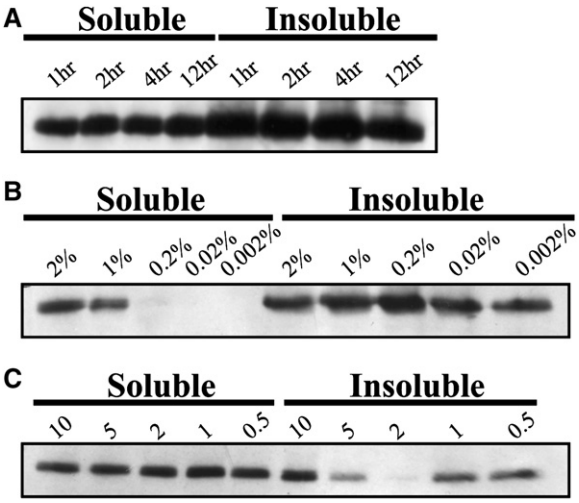

Figure 2. Optimization of ABCG2^{R482G} Solubilization by FC-16

(A) Membranes containing ABCG2^{R482G} were solubilized with 1% FC-16 at a protein concentration of 10 mg·ml^{-1} for 1 hr, 2 hr, 4 hr, and 12 hr at 4°C. Insoluble material and soluble proteins were assessed for the presence of ABCG2^{R482G} as described in Figure 1.

(B) Membranes containing ABCG2^{R482G} were solubilized with varying concentrations of FC-16 (0.002%–2% w/v) at a protein concentration of 10 mg·ml^{-1}. Solubilization was undertaken for 60 min at 4°C, and efficiency was assessed as described above.

(C) ABCG2^{R482G} solubilization efficiency was assessed by using varying concentrations (0.5–10 mg·ml^{-1}) of membrane protein with 1% (w/v) FC-16. Solubilization was undertaken for 60 min at 4°C, and efficiency was assessed as described above.

On the basis of these results, FC-16 was selected for further screens.

Optimization of Solubilization of ABCG2^{R482G}

The solubilization efficiency of FC-16 was investigated by time course solubilization trials. This demonstrated (Figure 2A) that, at 10 mg·ml^{-1} crude membrane protein, 1% FC-16, a 60 min solubilization at 4°C provided maximal solubilization. To identify the minimum amount of detergent required for efficient extraction of ABCG2^{R482G}, the concentration of the detergent was varied from 0.002% (4× CMC) to 2% with 10 mg·ml^{-1} crude membranes (Figure 2B). Extraction was only possible at concentrations of 2% and 1%, indicating that the protein was highly intransigent to extraction at low detergent concentrations. As 2% FC-16 gave slightly more extraction, the concentration of the detergent was fixed and the protein concentration varied from 10 mg·ml^{-1} to 0.5 mg·ml^{-1} (Figure 2C). This indicated that 2 mg·ml^{-1} crude membranes, 2% FC-16 were the optimal conditions for the solubilization of ABCG2^{R482G}.

Purification Scheme for FC-16-Soluble ABCG2^{R482G}

Solubilized membranes were analyzed by immobilized metal affinity chromatography (IMAC) (Figure 3A). However, the protein interacted weakly with the Ni^{2+}-NTA resin and was observed to elute at a relatively low (80 mM) imidazole concentration. Immunoblot analysis of the unbound material (not shown) indicated that the protein was binding with high efficiency to resin, albeit weakly. The amino-terminal His tag was not proteolytically cleaved since the eluted protein retained antihexahistidine monoclonal antibody reactivity. The peak elution fractions (Figure 3A, lanes 5–10) contained impurities and required an additional purification step.

ABCG2^{R482G}-containing fractions were concentrated and then equilibrated in a 20 mM NaCl buffer. The anion (MonoQ) exchange served as a pass-through purification step, as the majority of ABCG2^{R482G} eluted and the contaminating protein species bound (Figure 3B). The unbound ABCG2^{R482G} was concentrated and purified further by gel permeation chromatography (Figures 3C and 3D). SDS-PAGE analysis of the peak fractions showed that the sample was purified to homogeneity. The chromatographic trace shows a single species eluting from the column, indicating that ABCG2^{R482G} had purified in a single oligomeric state. Comparison to soluble molecular mass standards (Figure 3D, inset) was performed, and an apparent molecular mass of 430 kDa was determined.

Monomeric ABCG2^{R482G}, as observed on SDS-PAGE, is ~70 kDa. However, the minimal functional quaternary structure for a half-transporter would be dimerization with a cognate partner. Removal of reductants from SDS-PAGE has been a common approach for observing dimerization. Thus, gel permeation chromatography was performed in the presence of 5 mM TCEP, a strong reducing agent, in order to determine if ABCG2^{R482G} monomers could be observed (data not shown). Addition of TCEP failed to alter the elution profile of ABCG2^{R482G}, indicating that its oligomeric state was highly stable and could not be disrupted at this stage. Removal of reductants from SDS-PAGE did not lead to the detection of any dimeric species (data not shown).

Gel permeation chromatography is a poor technique for the determination of membrane proteins' molecular mass due to their aberrant migration compared to soluble protein standards (Schagger, 2003). Thus, BN-PAGE was performed as an alternative method by which the size of the oligomeric ABCG2^{R482G} complex could be analyzed (Figure 4). This technique gave a single band that, when compared to soluble protein standards, had a molecular mass of ~600 kDa.

Drug Binding to Detergent-Solubilized, Purified ABCG2^{R482G}

The integrity of function of detergent-soluble, purified ABCG2^{R482G} was assessed by measuring the binding of known substrates to the protein. ATPase activity was not measured since the protein was in a detergent-soluble, rather than a reconstituted, state. [^{125}I]Iodoarylazidoprazosin ([^{125}I]IAAP) was used to photoaffinity label ABCG2^{R482G} since it has previously been demonstrated to stimulate ATP hydrolysis by the protein (Ozvegy et al., 2001). Figure 5A (lane i) demonstrates that [^{125}I]IAAP was able to specifically photolabel the purified protein. Moreover, the binding of [^{125}I]IAAP was displaced by a number of known substrates of ABCG2^{R482G}, including prazosin, daunomycin, doxorubicin, and Hoechst33342 (Figure 5A). Figures 5B and 5C demonstrate full dose-response analysis of the specific [^{125}I]IAAP displacement by both prazosin and Hoechst33342. These data show that purified ABCG2^{R482G} retained the ability to interact with substrates and verified the fidelity of the samples after chromatography. Purified ABCG2^{R482G} also

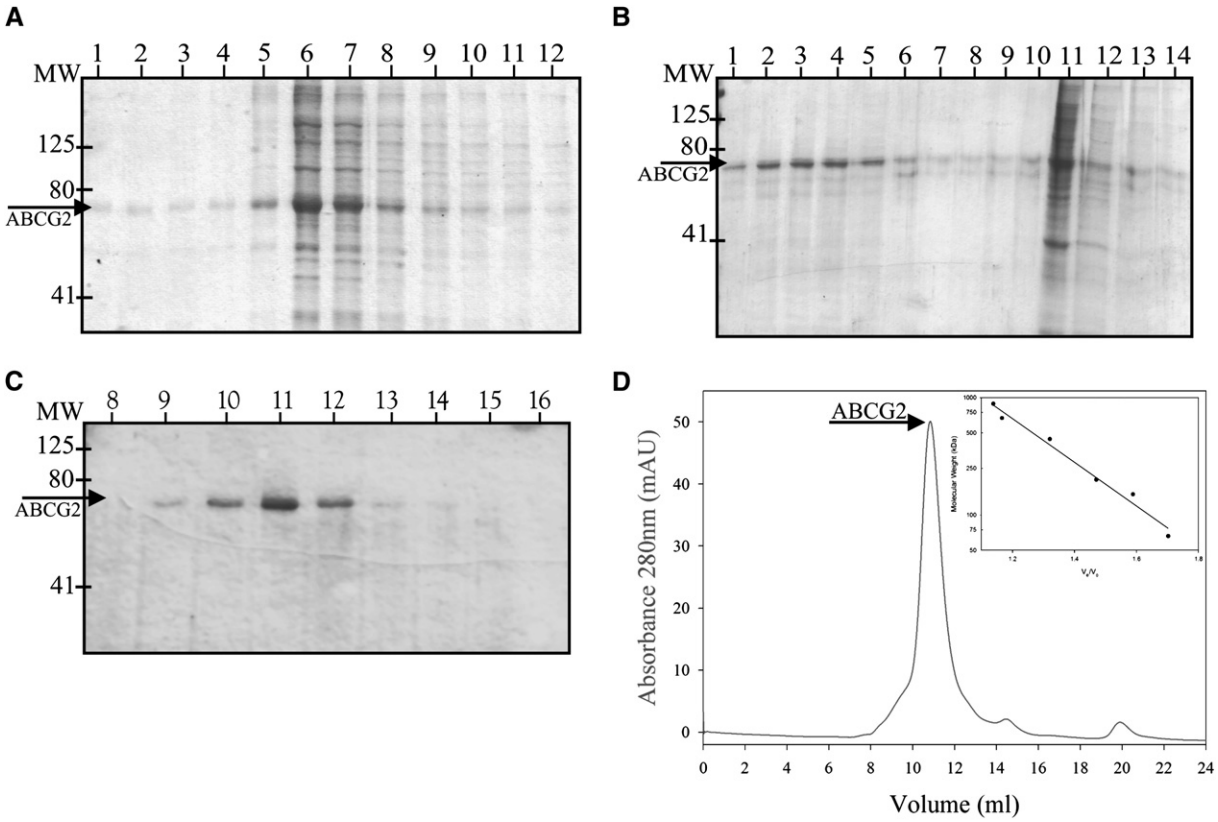

Figure 3. Purification Scheme for Detergent-Soluble ABCG2^{R482G}

FC-16-solubilized ABCG2^{R482G} was subjected to a three-stage purification scheme. Fractions containing protein are shown with PAGE-Blue-stained SDS-PAGE.

(A) Fractions obtained from IMAC. Lanes 1–4 show the 60 mM imidazole wash step, and lanes 5–12 show the specific elution of ABCG2^{R482G} at 200 mM imidazole.

(B) Anion exchange chromatography. The majority (>85%) of ABCG2^{R482G} was observed to elute in the unbound fractions (lanes 1–6) at 20 mM NaCl, while a proportion of ABCG2^{R482G} was observed to elute along with the majority of the impurities when the NaCl concentration was increased to 500 mM (lanes 10–14).

(C and D) Gel permeation chromatography. (C) Samples corresponding to elution volumes of 8–16 ml are shown, and the (D) corresponding 280 nm UV trace and the ABCG2^{R482G}-containing fractions are indicated. The inset in (D) shows the calibration curve of soluble marker proteins.

displayed low-level ATPase activity (data not shown) that was stimulated 1.5- to 2-fold by prazosin. The levels of activity were low, presumably because the protein was not reconstituted into lipid bilayers, a consistent observation for other ABC transporters (Callaghan et al., 1997; Modok et al., 2004).

Structural Analyses of the ABCG2^{R482G} Protein

Figure 6A shows a typical area of a micrograph of cryonegatively stained FC-16-solublized ABCG2^{R482G}. This shows that ABCG2^{R482G} forms uniform, large (~170 Å in diameter) particles with a size consistent with an oligomeric transporter complex. Projections of low-contrast complexes could be identified from the field of view (Figure 6A, boxes), with the most identifiable particle presenting a square/squared ring with a width of ~170 Å and a stained central region 60 Å in diameter. Other projections were rectangular in shape (~140 × 170 Å) and sometimes had noticeable bilateral symmetry. The population of complexes was homogeneous and generally nonaggregated, although some closely packed particles could be occasionally found and were not used in the single-particle analysis.

EM data collected under cryonegatively stained conditions (n = 7840) were analyzed and, when using reference-free classification, yielded a variety of projection classes, as shown in Figure 6B. Several classes had a noticeable 4-fold rotational symmetry, while other classes exhibited rounded rectangles with a more prominent bilateral symmetry, representing projections toward the top and side views of the complex, respectively. Other class averages represented various intermediate orientations between the top and side view projections (Figure 6B). The reference-free classification suggested that the particles were in a range of orientations under the preservative conditions, and that they were appropriate for 3D structure determination with cross-common lines projection matching (Ludtke et al., 1999).

Rotational power analysis (Figure 7B, inset) of the unsymmetrized projection classes showed strong correlation peaks for C2 and C4 rotational symmetries for several classes, as well as a weaker C8 peak. C2 symmetry would suggest a dimeric arrangement of ABCG2^{R482G} dimers, but the volume of the ABCG2^{R482G} complex (3,200,000 Å^3) is almost twice that required for four ABCG2^{R482G} subunits (~400 kDa), which argues against

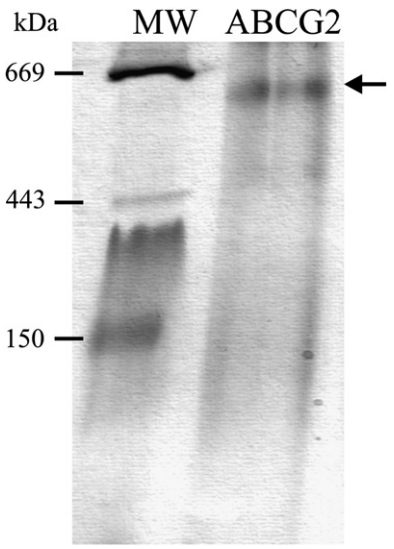

Figure 4. ABCG2^{R482} BN-PAGE

Purified ABCG2^{R482G} (5 μg) was analyzed by 4%–21% BN-PAGE. Soluble molecular mass standards are shown for size comparison, and ABCG2 is indicated by the arrow.

this arrangement. The calculations are based on the assumption of a protein density of 0.73cm^3/g (Collins et al., 2004). Biochemical considerations and the weaker C8 versus C4 peak in the power analysis (Figure 6B) suggested a tetramer of dimers, rather than a ring of eight monomers, as the likely configuration of the particles. Moreover, a higher-symmetry (C8) structure would be readily identifiable in a 3D map in which C4 symmetry had been imposed, hence the application of C4 symmetry.

Comparison of back projections of the final C4 structure with the corresponding averages generated from the unsymmetrized raw data showed excellent correlation (Figure 6C). The final resolution of the 3D structure was estimated at ~18 Å by using a FSC = 0.5 criterion (Figure 6D), and vector matrix analysis (Figure 6B, inset) revealed that the most populated classes used through the sampling were clustered around the central regions of the asymmetric triangle, although no significant gaps or missing projections were found. Viewed along the C4 rotational axis, the ABCG2^{R482G} oligomer has an obvious square or four-lobed shape. Viewed from the side, the ABCG2^{R482G} complex has an appearance similar to an upturned stool with stumpy legs on one side (Figure 7A). The structure has a width along the edge of the square of 150 Å, a corner-to-corner width of 180 Å, and a height of 145 Å. The structure suggests that the tetrameric particles are likely to be formed by four transporters, each formed by two ABCG2^{R482G} peptides. To aid in the interpretation of the structure, we used a homology model of a full-length ABC transporter of similar mass to a homodimeric ABCG2^{R482G} (Stenham et al., 2003) (Figures 7A and 7C). Manual placement of variable copies of the model within the 3D map (Figure 7C) confirmed that four ABCG2^{R482G} homodimers could be fitted almost exactly within the density map. Comparison of correlation coefficients also suggested a significantly better fit with the NBDs located at the bottom of the structure, as shown in Figure 7C, rather than at the top. An interesting aspect of the interpretation of the structure as shown in Figure 7C is that it suggests that the quaternary structure of the complex is stabilized by molecular contacts between the NBDs via tight packing.

Discussion

Gel permeation chromatography, nondenaturing electrophoresis, and EM structural analyses of the multidrug transporter ABCG2^{R482G} all reveal a stable quaternary structure of the protein subunits after detergent solubilization. Based on data from the majority of ABC transporters, it is highly likely that the minimal functional unit of ABCG2^{R482G} is a dimer; however, the biophysical analyses presented here indicate that ABCG2^{R482G} forms an oligomer that is probably arranged as a tetramer of dimers. The cryonegative staining technique has been used here because the high contrast imparted by the molybdate ions allows for an efficient classification of the single particles, while the microscopy conditions (presence of trehalose, neutral pH, low temperature) are likely to preserve the native structure of the protein (De Carlo et al., 2002; El-Bez et al., 2005). Classification into characteristic projection classes allows for the subsequent, nonsubjective analysis of symmetry, which has strongly indicated a C4 rotational symmetry. This concurs with the apparent molecular mass obtained by BN-PAGE. Finally, it was possible to dock four copies of a homology model for an ABC transporter almost exactly into the density available in the 3D map. In summary, these various data point to the presence of a tetrameric arrangement, which is likely to be composed of (four) homodimeric ABCG2^{R482G} units.

ABCG2^{R482G} expressed in insect cells was difficult to solubilize by conventional mild nonionic and zwitterionic detergents. The most effective detergents to achieve solubilization of ABCG2^{R482G} were the long-chain Fos-choline derivatives. This finding was in contrast to similar investigations with ABCB1, which was readily solubilized from membranes by mild detergents (Taylor et al., 2001). However, they reported that a considerable proportion (~40%–50%) of the ABCB1 was not extractable. It has become increasingly evident that many ABC transporters are resistant to extraction from insect cell membranes. ABCA4 (unpublished data) is not extracted by detergents such as β-OG and DDM, yet the lysophospholipid analogs FC-14 and -16 are efficient extractors. In addition, Ramjeesingh et al. (1997) reported that CFTR extraction from insect cells required PFO for solubilization, and that this necessitated a long incubation time. An additional technical difficulty encountered with ABCG2^{R482G} was the relatively low binding affinity to the IMAC resin compared to that reported for ABCB1 (Taylor et al., 2001), SUR1 (Mikhailov et al., 2005), and ABCC1 (Chang et al., 1997). This observation suggests that the His tag of ABCG2^{R482G} is at least partially occluded by the structure, which may be related to the quaternary structure reported here.

Functional data based on the catalytic cycle of ABC transporters strongly suggest that two NBDs are required to power drug translocation; i.e., the minimal functional unit for ABCG2 should be a homodimer. Previous studies of ABCG2 have indicated a range of nonspecified and undetermined oligomeric states after

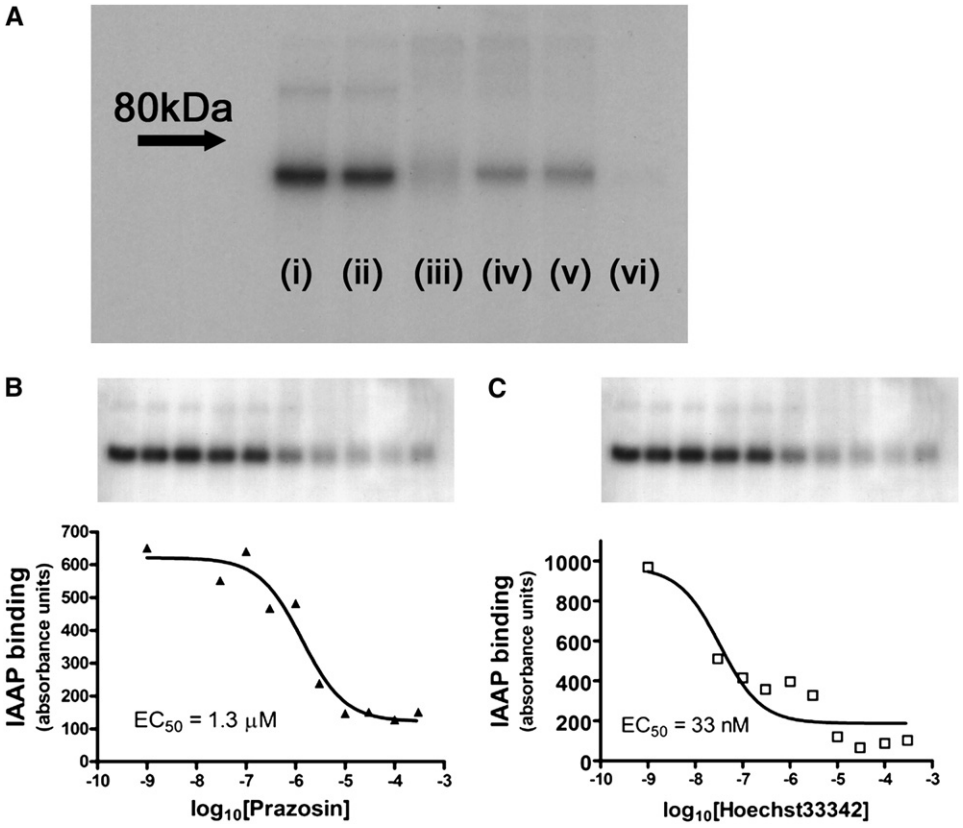

Figure 5. Drug Binding by Detergent-Soluble ABCG2^{R482G}

(A–C) Purified ABCG2^{R482G} (1 μg) was incubated with [^{125}I]IAAP as described in the Experimental Procedures. Samples were resolved by 8% SDS-PAGE, and fixed gels were imaged by autoradiography. (A) Substrate additions were: lane i, no addition (i.e., IAAP alone); ii, DMSO (solvent control); iii, prazosin (300 μM); iv, doxorubicin (100 μM); v, daunomycin (100 μM); vi, Hoescht33342 (3 μM). (B and C) ABCG2^{R482G} was incubated in the presence of varying concentrations (1 nM–300 μM) of (B) prazosin or (C) Hoechst33342. The autoradiograms (upper panels) demonstrate the ABCG2^{R482G} crosslinked with [^{125}I]IAAP, and the amount of labeling was quantified by densitometry (lower panels) and was analyzed with nonlinear regression.

extraction with TX-100 and analysis by gel filtration and density gradient centrifugation (Bhatia et al., 2005; Xu et al., 2004). Gel permeation chromatography of ABCG2^{R482G} indicated a single oligomeric species and a consistent molecular mass of 430 kDa. Allowing for a detergent contribution, this could be interpreted as evidence for a dimer of dimers. However, these data are probably misleading, as gel permeation chromatography can be a poor analytical tool for membrane protein mass determination (Ford et al., 1990); its benefit in the present study was to demonstrate the homogeneity of protein preparations. Based on the molecular mass of monomeric ABCG2^{R482G}, a tetramer of dimers structure would be predicted to have a molecular mass of ~560 kDa protein plus a detergent shell of unknown mass, possibly 50–100 kDa. This would be consistent with the ~600 kDa molecular mass observed by BN-PAGE. Some density in the 3D map around the TMDs may arise due to a band of detergent around the exposed hydrophobic residues, although the detergent shell will vary from one particle to another, and hence may be at least partially averaged out by the analysis.

It is difficult to discriminate whether the observed tetramer of dimers is the native in vivo state for ABCG2^{R482G} in biological membranes or a by-product of the purification procedure. The oligomeric state of functionally active, purified membrane proteins can depend on the detergent used in the purification (Ford et al., 1990). Similarly, overexpression of the recombinant protein can also facilitate quaternary interactions. Observation of ABCG2^{R482G} interaction with the substrates prazosin and Hoechst33342 indicates that the purified protein has retained function. Moreover, there are numerous reports of ABC transporters associating in various oligomeric states. For example, Pdr5p, the major multidrug exporter in *Saccharomyces cerevisiae*, was observed by EM as a dimer of dimers. Atomic force microscopy of another ABC protein, CFTR, expressed in native "inside-out"-oriented membrane patches (Schillers et al., 2004), reports a similar dimeric arrangement, as did previous freeze-fracture EM studies (Eskandari et al., 1998). However, detergent-solubilized CFTR (Awayn et al., 2005) may also adopt a dimeric organization, depending on the purification detergent. YvcC, which, like ABCG2^{R482G}, is a "half-transporter," forms an unusual ring of ABC transporters after detergent removal, and each individual transporter subunit is oriented perpendicular to the rotational axis of the ring (Chami et al., 2002). Recently, a tetrameric organization of the SUR1-Kir6.2 protein has been observed by EM (Mikhailov et al., 2005), and an arrangement of the NBDs of SUR1 that is almost identical to those predicted

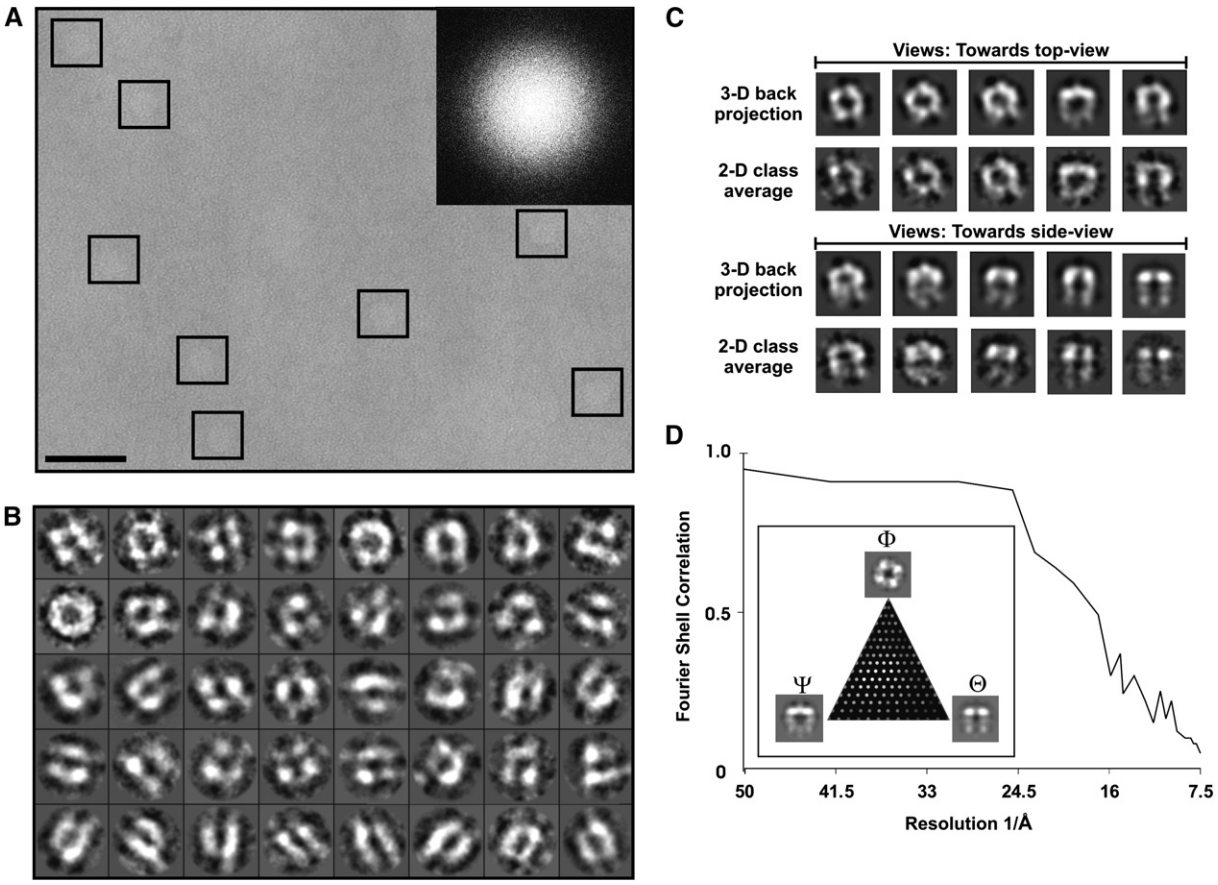

Figure 6. Cryonegatively Stained Electron Microscopy and Single-Particle Analysis of ABCG2^{R482G}

(A) Low-contrast individual cryonegatively stained oligomeric complexes are shown in boxes. The image was recorded at ~3.0 μm underfocus and has been CTF corrected and low-pass filtered to 20 Å. The inset shows the FFT of the EM data with concentric Thon rings extending to the edge of the FFT and a theoretical resolution of 6.2 Å. The scale bar is 500 Å.

(B) Montage of some of the unsymmetrized ABCG2^{R482G} class averages produced by reference-free classification and averaging of particles imaged by cryonegatively stained EM. Data were CTF corrected and low-pass filtered (25 Å) prior to classification. Each individual box is 237 × 237 Å, and the circular mask applied has a diameter of 211 Å.

(C) Correlation of experimental projection averages to the final 3D structure. The lower row shows a selection of the experimental analyses (no symmetry imposed) with corresponding back projections from the final C4-symmetrized 3D structure (upper panels). Boxes are 237 × 237 Å.

(D) FSC plot calculated by comparison of two separate 3D structures calculated by splitting the data set into two. The two structures were thresholded at 1.05σ above the mean density, and C4 symmetry was applied (Ludtke et al., 1999). The inset shows the distribution of class averages used to calculate the 3D structure between Euler angles ψ, φ, and ϕ.

for ABCG2^{R482G} herein is seen. The tetrameric association of SUR1 proteins with a tetramer of K_{ATP} channels is in agreement with functional information on the oligomeric state (Clement et al., 1997).

Recent pharmacological data with ABCG2^{R482G} support a potential functional role for the oligomeric association of protein subunits. Radioligand-binding data indicate that drug interaction with ABCG2^{R482G} in native membranes is characterized by the presence of multiple and pharmacologically distinct binding sites. Moreover, drug-binding sites display a complex allosteric communication. One possible explanation is allosteric interaction between multiple sites within the functional ABCG2^{R482G} dimer; however, these effects may also be achieved by interaction between multiple dimers of the protein within a higher oligomer.

To our knowledge, the data presented here provide the first 3D information on the oligomeric structure of ABCG2^{R482G}, which belongs to the subsection of ABC transporters with a "reverse topology." A robust and efficacious purification procedure has been established that will enable further biochemical characterization of the pharmacophoric properties via reconstitution of the protein. The stable oligomeric association provides us with a means to pursue further structural studies with cryonegative-stained electron microscopy of samples in thin vitreous ice.

Experimental Procedures

Materials

Octyl-β-glucoside (β-OG) and Zwittergent (ZW) 3-16 were purchased from Merck Biosciences (Nottingham, UK), CHAPS was purchased from Sigma (Poole, UK), and pentadecafluoro-octanoic acid (PFO) was purchased from Fluorochem (Old Glossop, UK). Foscholine (FC-) (8, 12, 14, and 16), cyclofos (CF-) (2 and 5), cymal (CY-) (2 and 4), dodecyl-β-maltoside, dodecyl-β-maltoside (DDM), and lauryldimethylamine oxide (LDAO) were obtained from Anatrace (Maumee, Ohio). The FPLC columns Histrap, MonoQ 5/50, and Superdex S200 were purchased from GE Healthcare (Chalfont St. Giles, UK).

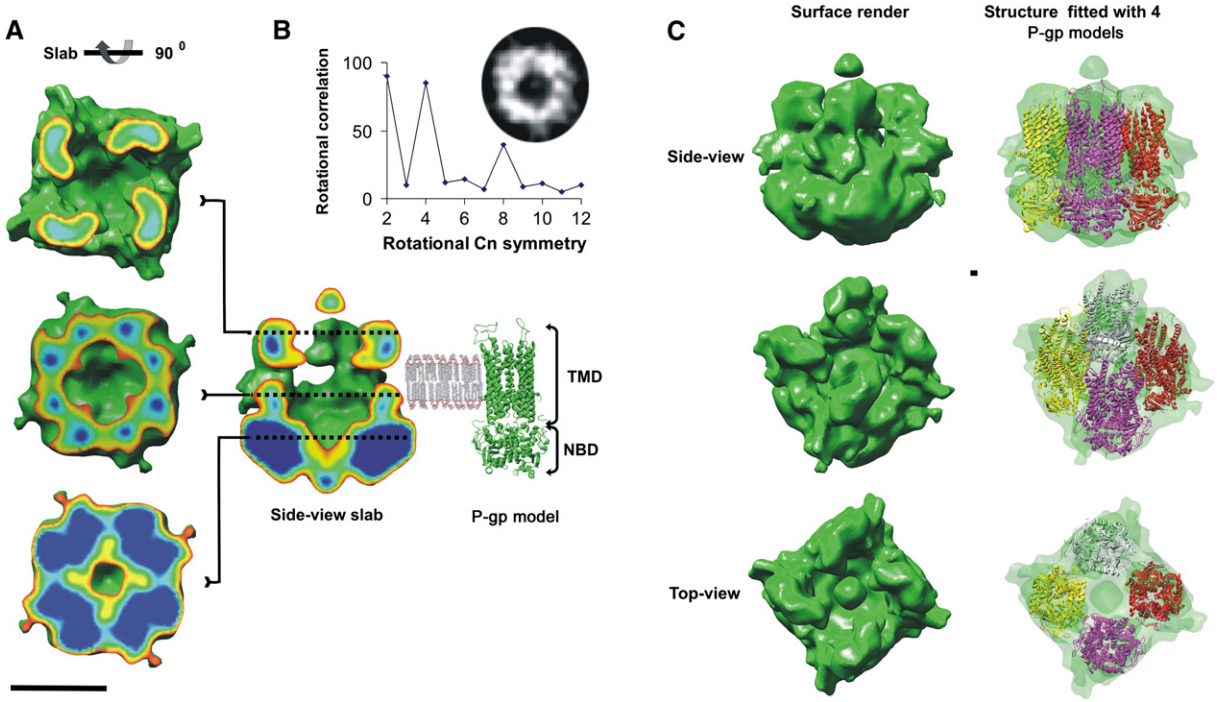

Figure 7. 3D Structure and Interpretation

(A) Sections through the height of the ABCG2^{R482G} complex (i.e., slices perpendicular to the C4 axis and displaying bilateral symmetry) are shown on the left, with corresponding positions of the slice planes indicated in the side view slab in the center. An indication of the position of the membrane with respect to the side view is indicated on the right, as predicted from the positioning of the homology model (far right). Slabbed sections have the following display thresholds: green, 1.05σ; red, 2σ; orange, 2.5σ; yellow, 3σ; cyan, 3.5σ; and blue, 4σ. The volume was low-pass filtered to 18 Å resolution, and a high-pass Fermi filter was applied to boost higher-resolution frequency information. The scale bar is 100 Å.

(B) Rotational power analysis of a typical class average displaying some rotational symmetry (Collins et al., 2003). The class average (representing 110 particles) was low-pass filtered to 25 Å resolution.

(C) Surface structure and interpretation. Surface of the ABCG2^{R482G} complex (left column), as viewed from the side (upper row), the top (lower row), and an intermediate view (center row). Corresponding views displaying the fitting with four copies of the homology model are shown in the right-hand column.

Generation of Recombinant Baculovirus Encoding N-His$_6$-ABCG2^{R482G}

An ABCG2 cDNA-containing plasmid, encoding glycine at position 482 (ABCG2^{R482G}), was obtained from Dr. T. Litman (University of Copenhagen). Oligonucleotide primers (5′-CTAGACTCGAGCGGCGCCATGTCTTCCAGTAATG-3′ and 3′-CTTGGTACCGAGCGCGGCCGCCTAAGAATATTTTTTAAG-5′) were employed to amplify the cDNA and add 5′ KasI and 3′ NotI restriction sites (underlined). The resultant PCR product was digested and subcloned into the pFastBac-HTC vector (Invitrogen), generating a cDNA that encodes an N-terminal extension to ABCG2^{R482G} of MSYY*HHHHHH* DYDIPTT **ENLYFQGA**MSSSN, where the affinity tag is italicized, the TEV-protease cleavage site is in bold, and the first five amino acids of the open reading frame of ABCG2^{R482G} are underlined. The fidelity of PCR was confirmed by DNA sequencing of this resultant construct. This vector was transformed into chemically competent DH10Bac *E. coli* cells. Putative recombinant bacterial colonies were restreaked to ensure no contamination by nonrecombinant bacteria and were further screened by PCR, after isolation of high-molecular weight bacmid DNA. Insect cells (Sf9, 9 × 10^5 cells per 30 mm dish) were transfected with recombinant bacmid DNA (3 μg DNA, 6 μg lipofectin) to produce an initial viral titer suitable for further amplification as previously described (Taylor et al., 2001).

Expression of ABCG2^{R482G} and Isolation of Insect Cell Membranes

The *Trichoplusia ni* (High Five) cell line was routinely used for the expression of ABCG2^{R482G} and was maintained in shaking suspension cultures as previously described (Rothnie et al., 2004). Crude membrane preparations were isolated as previously described (Taylor et al., 2001), with the exception that buffers contained 20 mM MOPS (pH 7.4), 200 mM NaCl, and 0.25 M sucrose.

ABCG2^{R482G} Solubilization Trials

Membranes were solubilized in 20 mM MOPS (pH 7.4), 200 mM NaCl, 1.5 mM $MgCl_2$, 20% glycerol buffer containing, minimally, 2× CMC of the detergents. Protease inhibitors were maintained throughout the solubilization and purification. Solubilizations were incubated for 60 min at 4°C (except for PFO, which was incubated at 20°C) and were mixed, and the soluble fractions were then isolated by ultracentrifugation (100,000 × g, 60 min). Insoluble material was resuspended in 10% SDS, and equivalent protein concentrations were analyzed by 10% SDS-PAGE and immunoblotting. Immunoblotting analysis was performed by using an anti-6xHis HRP-conjugated monoclonal antibody from R & D (Abingdon, UK) and was visualized by ECL.

Chromatographic Isolation of ABCG2^{R482G}

Solubilized protein was analyzed by immobilized metal affinity chromatography (IMAC) by using a HisTrap column with a stepwise gradient from 40 mM to 800 mM imidazole. Partially purified protein was concentrated by using centrifugal concentrators with a molecular weight (MW) cutoff of 100 kDa (Millipore, UK). The concentrated sample was diluted 15-fold in 20 mM MOPS (pH 7.4), 20 mM NaCl, 1.5 mM $MgCl_2$, 20% glycerol, 0.1% Fos-choline-16 (FC-16) and was loaded onto a MonoQ 5/50 column with a step gradient from 20 mM NaCl to 500 mM NaCl. Gel permeation chromatography was performed in 20 mM MOPS (pH 7.4), 50 mM NaCl, 1.5 mM $MgCl_2$, 20% glycerol, 0.1% FC-16 on a Superdex S200 10/30 column at a flow rate of 0.3 ml.min^{-1}. Soluble molecular mass standards

Table 1. Cryo-Electron Microscopy and Image Analysis Information Used for the Single-Particle 3D Reconstructions

	Cryonegatively Stained Data	Negatively Stained Data
Microscope	Philips CM200 FEG	Tecnai CM10
Mode	TEM low dose at <100K	TEM low dose
Operating voltage	200 kV	100 kV
Micrograph film	—	Kodak SO-163
Digitization	Gatan 4Kx4K CCD camera	UMAX 3000
Spot size	5	3
Dose (electron/Å^2)	<20	<40
Calibrated magnification	38,000	43,000
Å/pixel at specimen level	3.1	3.7
Defocus range (Å)	−12,000 to −35,000	−2,000 to −5,000
Selection box (Å)	237	300
Total particles	7,840	2,240
Particle classes	131	60
Reconstruction mask radius (Å)	220	200
Spatial resolution, FSC = 0.5 (Å)	18	22

used were from the High Molecular Mass Calibration kit from Sigma (Poole, UK). Retention time of the molecular mass standards was analyzed as described (Andrews, 1964; Whitaker, 1963). BN-PAGE analysis was performed as described by Schagger et al. (1994). Protein determination was performed by using the BioRad D_c Brad kit. BN- and SDS-PAGE gels were stained with PAGE-Blue from Helena Biosciences (Gateshead).

Drug Binding by ABCG2^{R482G}

ABCG2^{R482G} (1 μg) was incubated with [^{125}I]iodoarylazidoprazosin ([^{125}I]IAAP) (6 nM) in the absence or presence of varying concentrations of known substrates for 2 hr at 20°C in the dark. Samples (30 μl) were then incubated for 10 min on ice and irradiated at 260 nm (100W) for 8 min on ice. After irradiation, 10 μl of 4× Laemmli buffer was added to the samples, which were then analyzed by 8% SDS-PAGE. The gels were washed in water and fixed in 25% (v/v) isopropanol and 10% (v/v) acetic acid. Fixed gels were dried and exposed to photographic film. Where competing drugs were used, the compounds were added from concentrated stocks in DMSO, and the solvent concentration was maintained at below 1% (v/v). Drugs were added at concentrations between 30 nM and 1 mM.

Cryonegative and Negative Staining of ABCG2^{R482G}

Carbon-coated copper grids (400 mesh) were glow discharged for 30 s and placed on the surface of a 10 μl droplet of sample containing 100 μg.ml^{-1} ABCG2^{R482G} for 2 min. Cryonegative staining was performed as described by Adrian et al. (1998).

Image Processing and Structure Calculation from ABCG2^{R482G} EM Data

Data were processed in a subsequent manner (Table 1). Detergent-solubilized complexes were interactively selected by using BOXER and were contrast normalized. The contrast transfer function (CTF) for each micrograph was determined by using CTFIT (Ludtke et al., 1999), and phase corrections were applied. A set of reference-free class averages was then generated. Following established strategies, a preliminary 3D model was determined from class averages that represented distinct views of the ABCG2^{R482G} complex. Relative orientations of the characteristic views were determined by using a Fourier common-lines routine, and resulting averages were combined to generate the preliminary 3D model. The structure was refined by using C4 symmetry, using eight rounds of iterative projection matching, with each refinement assessed by examining convergence by comparison of the Fourier Shell Correlation (FSC) of the 3D models generated from each iteration. The final 3D volume was fully converged after six rounds of iterative refinement, and resolution was determined by FSC analysis. A homology model of ABCG2 (J.D. Campbell, personal communication) based on an atomic-scale structural model of ABCB1 (Stenham et al., 2003) was docked in the 3D map by using Chimera. After fitting four copies of the model, a 3D map at the same resolution as the experimental structure was generated from the model tetramer. This map was then aligned rotationally and translationally against the experimental structure, and an FSC was calculated between the two aligned maps. A similar procedure was carried out with the whole model rotated through 180° so that the NBDs were facing in the opposite direction.

Acknowledgments

This research was funded by a Cancer Research UK Program grant (SP1861/0401). I.D.K. was supported by a New Lecturer's Fund grant from the University of Nottingham. The contribution of ABCG2^{R482G} cDNA by Dr. T. Litman from the University of Copenhagen is greatly appreciated.

Received: June 22, 2006
Revised: August 4, 2006
Accepted: August 8, 2006
Published: November 14, 2006

References

Adrian, M., Dubochet, J., Fuller, S.D., and Harris, J.R. (1998). Cryonegative staining. Micron *29*, 145–160.

Andrews, P. (1964). Estimation of the molecular weights of proteins by Sephadex gel-filtration. Biochem. J. *91*, 222–233.

Awayn, N.H., Rosenberg, M.F., Kamis, A.B., Aleksandrov, L.A., Riordan, J.R., and Ford, R.C. (2005). Crystallographic and single-particle analyses of native- and nucleotide-bound forms of the cystic fibrosis transmembrane conductance regulator (CFTR) protein. Biochem. Soc. Trans. *33*, 996–999.

Bhatia, A., Schafer, H.J., and Hrycyna, C.A. (2005). Oligomerization of the human ABC transporter ABCG2: evaluation of the native protein and chimeric dimers. Biochemistry *44*, 10893–10904.

Callaghan, R., Berridge, G., Ferry, D.R., and Higgins, C.F. (1997). The functional purification of P-glycoprotein is dependent on maintenance of a lipid-protein interface. Biochim. Biophys. Acta *1328*, 109–124.

Chami, M., Steinfels, E., Orelle, C., Jault, J.M., Di Pietro, A., Rigaud, J.L., and Marco, S. (2002). Three-dimensional structure by cryo-electron microscopy of YvcC, an homodimeric ATP-binding cassette transporter from *Bacillus subtilis*. J. Mol. Biol. *315*, 1075–1085.

Chang, X.B., Hou, Y.X., and Riordan, J.R. (1997). ATPase activity of purified multidrug resistance-associated protein. J. Biol. Chem. *272*, 30962–30968.

Chen, Z.S., Robey, R.W., Belinsky, M.G., Shchaveleva, I., Ren, X.Q., Sugimoto, Y., Ross, D.D., Bates, S.E., and Kruh, G.D. (2003). Transport of methotrexate, methotrexate polyglutamates, and 17β-estradiol 17-(β-D-glucuronide) by ABCG2: effects of acquired mutations at R482 on methotrexate transport. Cancer Res. *63*, 4048–4054.

Clark, R., Kerr, I.D., and Callaghan, R. (2006). Multiple drug binding sites on the R482G isoform of the ABCG2 transporter. Br. J. Pharmacol., in press. Published online September 18, 2006. 10.1038/sj.bjp.0706904.

Clement, J.P., IV, Kunjilwar, K., Gonzalez, G., Schwanstecher, M., Panten, U., Aguilar-Bryan, L., and Bryan, J. (1997). Association and stoichiometry of K(ATP) channel subunits. Neuron *18*, 827–838.

Collins, R.F., Ford, R.C., Kitmitto, A., Olsen, R.O., Tonjum, T., and Derrick, J.P. (2003). Three-dimensional structure of the *Neisseria meningitidis* secretin PilQ determined from negative-stain transmission electron microscopy. J. Bacteriol. *185*, 2611–2617.

Collins, R.F., Frye, S.A., Kitmitto, A., Ford, R.C., Tonjum, T., and Derrick, J.P. (2004). Structure of the *Neisseria meningitidis* outer membrane PilQ secretin complex at 12 Å resolution. J. Biol. Chem. *279*, 39750–39756.

De Carlo, S., El-Bez, C., Alvarez-Rua, C., Borge, J., and Dubochet, J. (2002). Cryo-negative staining reduces electron-beam sensitivity of vitrified biological particles. J. Struct. Biol. *138*, 216–226.

El-Bez, C., Adrian, M., Dubochet, J., and Cover, T.L. (2005). High resolution structural analysis of *Helicobacter pylori* VacA toxin oligomers by cryo-negative staining electron microscopy. J. Struct. Biol. *151*, 215–228.

Eskandari, S., Wright, E.M., Kreman, M., Starace, D.M., and Zampighi, G.A. (1998). Structural analysis of cloned plasma membrane proteins by freeze-fracture electron microscopy. Proc. Natl. Acad. Sci. USA *95*, 11235–11240.

Ford, R.C., Hefti, A., and Engel, A. (1990). Ordered arrays of the photosystem I reaction centre after reconstitution: projections and surface reliefs of the complex at 2 nm resolution. EMBO J. *9*, 3067–3075.

Graf, G.A., Yu, L., Li, W.P., Gerard, R., Tuma, P.L., Cohen, J.C., and Hobbs, H.H. (2003). ABCG5 and ABCG8 are obligate heterodimers for protein trafficking and biliary cholesterol excretion. J. Biol. Chem. *278*, 48275–48282.

Kage, K., Tsukahara, S., Sugiyama, T., Asada, S., Ishikawa, E., Tsuruo, T., and Sugimoto, Y. (2002). Dominant-negative inhibition of breast cancer resistance protein as drug efflux pump through the inhibition of S-S dependent homodimerization. Int. J. Cancer *97*, 626–630.

Litman, T., Jensen, U., Hansen, A., Covitz, K.M., Zhan, Z., Fetsch, P., Abati, A., Hansen, P.R., Horn, T., Skovsgaard, T., and Bates, S.E. (2002). Use of peptide antibodies to probe for the mitoxantrone resistance-associated protein MXR/BCRP/ABCP/ABCG2. Biochim. Biophys. Acta *1565*, 6–16.

Ludtke, S.J., Baldwin, P.R., and Chiu, W. (1999). EMAN: semiautomated software for high-resolution single-particle reconstructions. J. Struct. Biol. *128*, 82–97.

Mikhailov, M.V., Campbell, J.D., de Wet, H., Shimomura, K., Zadek, B., Collins, R.F., Sansom, M.S., Ford, R.C., and Ashcroft, F.M. (2005). 3-D structural and functional characterization of the purified KATP channel complex Kir6.2-SUR1. EMBO J. *24*, 4166–4175.

Mitomo, H., Kato, R., Ito, A., Kasamatsu, S., Ikegami, Y., Kii, I., Kudo, A., Kobatake, E., Sumino, Y., and Ishikawa, T. (2003). A functional study on polymorphism of the ATP-binding cassette transporter ABCG2: critical role of arginine-482 in methotrexate transport. Biochem. J. *373*, 767–774.

Modok, S., Heyward, C., and Callaghan, R. (2004). P-glycoprotein retains function when reconstituted into a sphingolipid- and cholesterol-rich environment. J. Lipid Res. *45*, 1910–1918.

Nakagawa, M., Schneider, E., Dixon, K.H., Horton, J., Kelley, K., Morrow, C., and Cowan, K.H. (1992). Reduced intracellular drug accumulation in the absence of P-glycoprotein (mdr1) overexpression in mitoxantrone-resistant human MCF-7 breast cancer cells. Cancer Res. *52*, 6175–6181.

Ozvegy, C., Litman, T., Szakacs, G., Nagy, Z., Bates, S., Varadi, A., and Sarkadi, B. (2001). Functional characterization of the human multidrug transporter, ABCG2, expressed in insect cells. Biochem. Biophys. Res. Commun. *285*, 111–117.

Ozvegy, C., Varadi, A., and Sarkadi, B. (2002). Characterization of drug transport, ATP hydrolysis, and nucleotide trapping by the human ABCG2 multidrug transporter. Modulation of substrate specificity by a point mutation. J. Biol. Chem. *277*, 47980–47990.

Polgar, O., Robey, R.W., Morisaki, K., Dean, M., Michejda, C., Sauna, Z.E., Ambudkar, S.V., Tarasova, N., and Bates, S.E. (2004). Mutational analysis of ABCG2: role of the GXXXG motif. Biochemistry *43*, 9448–9456.

Poruchynsky, M.S., and Ling, V. (1994). Detection of oligomeric and monomeric forms of P-glycoprotein in multidrug resistant cells. Biochemistry *33*, 4163–4174.

Ramjeesingh, M., Li, C., Garami, E., Huan, L.J., Hewryk, M., Wang, Y., Galley, K., and Bear, C.E. (1997). A novel procedure for the efficient purification of the cystic fibrosis transmembrane conductance regulator (CFTR). Biochem. J. *327*, 17–21.

Reyes, C.L., and Chang, G. (2005). Structure of the ABC transporter MsbA in complex with ADP.vanadate and lipopolysaccharide. Science *308*, 1028–1031.

Robey, R.W., Honjo, Y., van de Laar, A., Miyake, K., Regis, J.T., Litman, T., and Bates, S.E. (2001). A functional assay for detection of the mitoxantrone resistance protein, MXR (ABCG2). Biochim. Biophys. Acta *1512*, 171–182.

Rosenberg, M.F., Mao, Q., Holzenburg, A., Ford, R.C., Deeley, R.G., and Cole, S.P. (2001). The structure of the multidrug resistance protein 1 (MRP1/ABCC1). Crystallization and single-particle analysis. J. Biol. Chem. *276*, 16076–16082.

Rothnie, A., Storm, J., Campbell, J., Linton, K.J., Kerr, I.D., and Callaghan, R. (2004). The topography of transmembrane segment six is altered during the catalytic cycle of P-glycoprotein. J. Biol. Chem. *279*, 34913–34921.

Russ, W.P., and Engelman, D.M. (2000). The GxxxG motif: a framework for transmembrane helix-helix association. J. Mol. Biol. *296*, 911–919.

Schagger, H. (2003). Blue native electrophoresis. In Membrane Protein Purification and Crystallization: A Practical Guide, C. Hunte, G. von Jagow, and H. Schagger, eds. (London: Academic Press), pp. 49–51.

Schagger, H., Cramer, W.A., and von Jagow, G. (1994). Analysis of molecular masses and oligomeric states of protein complexes by blue native electrophoresis and isolation of membrane protein complexes by two-dimensional native electrophoresis. Anal. Biochem. *217*, 220–230.

Schillers, H., Shahin, V., Albermann, L., Schafer, C., and Oberleithner, H. (2004). Imaging CFTR: a tail to tail dimer with a central pore. Cell. Physiol. Biochem. *14*, 1–10.

Soszynski, M., Kaluzna, A., Rychlik, B., Sokal, A., and Bartosz, G. (1998). Radiation inactivation suggests that human multidrug resistance-associated protein 1 occurs as a dimer in the human erythrocyte membrane. Arch. Biochem. Biophys. *354*, 311–316.

Stenham, D.R., Campbell, J.D., Sansom, M.S., Higgins, C.F., Kerr, I.D., and Linton, K.J. (2003). An atomic detail model for the human ATP binding cassette transporter P-glycoprotein derived from disulfide cross-linking and homology modeling. FASEB J. *17*, 2287–2289.

Taylor, A.M., Storm, J., Soceneantu, L., Linton, K.J., Gabriel, M., Martin, C., Woodhouse, J., Blott, E., Higgins, C.F., and Callaghan, R. (2001). Detailed characterization of cysteine-less P-glycoprotein reveals subtle pharmacological differences in function from wild-type protein. Br. J. Pharmacol. *134*, 1609–1618.

Whitaker, J.R. (1963). Determination of molecular weights of proteins by gel filtration on sephadex. Anal. Chem. *35*, 1950–1953.

Xu, J., Liu, Y., Yang, Y., Bates, S., and Zhang, J.T. (2004). Characterization of oligomeric human half-ABC transporter ATP-binding cassette G2. J. Biol. Chem. *279*, 19781–19789.